DOI: 10.1007/s12541-012-0041-3

Direct Micro-joining of Flexible Printed Circuit and Metal Electrode by Pulsed Nd:YAG Laser

Mohd Idris Shah Ismail[1,#], Yasuhiro Okamoto[1], Akira Okada[1], Yoshiyuki Uno[1] and Kentaro Ueoka[1]

1 Graduate School of Natural Science and Technology, Okayama University, 3-1-1, Tsushima-naka, Kita-ku, Okayama, Japan, 700-8530
Corresponding Author / E-mail: idris@ntmlab.mech.okayama-u.ac.jp, TEL: +81-86-251-8038, FAX: +81-86-251-8039

KEYWORDS: Copper, Overlap welding, Pulse waveform, Pre-heating, Post-heating, Rest time

Laser micro-welding has proven to be a very successful tool for micro-joining in the electrical and electronic industries, where the miniaturization, the high strength and the high heat resistance are constantly requested. Recently, a flexible printed circuit (FPC) is expected as a new connection technology between electrical conductors according to the improvements of reliability and controllability with the diversification of the design concept. In this technology, it is required to weld a several tens μm thickness of FPC and a several hundreds μm thickness of metal electrode. This material combination accompanies the difficulty to control the welding phenomenon due to the differences of thermal property and heat capacity. As a good alternative, laser micro-welding has advantages of non-contact tool, low heat distortion and consistent weld integrity. In this study, the overlap welding of thin copper circuit on a polyimide film and a thick brass electrode was experimentally and numerically investigated by using a pulsed Nd:YAG laser. In addition, the shearing stress of overlap welding was evaluated with and without the control of pulse waveform, which can provide a well-directed controlling of the heat input with high energy density. The results showed that a porosity was observed as the major weld defect in the welding process without a pulse control. However, the appropriate controlled laser pulse configuration of micro-welding could remove the weld defects in the molten zone, improve the weld penetration stability and increase the weld strength. The potential benefits of controlled pulse waveform were discussed for the direct laser micro-welding process. It is clarified that the direct laser micro-welding of a thin copper circuit on a polyimide film and a thick brass electrode could be successfully achieved by appropriate controlled pulse waveform and heat input.

Manuscript received: June 20, 2011 / Accepted: October 4, 2011

1. Introduction

As one of the most important developments in manufacturing processes, machining operations can contribute to profitability significantly. The best techniques can result in low production costs and keep the competitiveness of products. The development of the direct joining method is important to major applications in the automobile and electronic fields. Among various joining techniques, it is well-known that the laser welding is an effective technique for joining thin metals because the laser beam has a high power density to melt metals easily at a high processing speed with a precise positioning.[1-3] Electronic industry is becoming increasingly interested in laser welding technology to joint electronic components. Starting from July 2006, the WEEE/RoHS laws in Europe forbids the usage of lead in solders, which is very harmful to the human body and the environment.[4,5] The laws gave impetus to the solder-free in the laser welding as a promising solution to replace the conventional joining technique.

A flexible printed circuit (FPC) is strongly expected as a connection component because of its high reliability for movable parts of electronic device. FPC has greatly contributed to make devices thinner, lighter and more compact. Copper and its alloys are some of the most versatile materials and widely used in the electrical and electronic components because of its high ability to conduct the energy and transmit the signals.[6] However, the high thermal conductivity of copper has a great influence on weldability.[7] In the welding process, the heat is rapidly conducted into the copper, which might lead to the incomplete fusion in the weldments. Moreover, the welding process of copper can be essentially described in the same way as that on other metals. However, the primary difficulty in the laser welding of copper is the crucial time to form the weld pool at the beginning of the process because of its high reflectivity and the high thermal conductivity, which makes it difficult to initiate a reliable welding process.[8] Furthermore, the main challenging in the laser welding of copper-alloy brass is the generation of porosity due to the evaporation of

alloyed zinc from a brass,[9] since the boiling point of zinc is lower than the melting point of copper. Therefore, the achievement of high reliability is mandatory for applying the laser welding technique in the industrial production lines.

In the laser micro-welding of high reflective materials, the use of a standard pulse profile is limited to weld the dissimilar metals of copper and brass in the overlap joint geometry, since the uncontrolled heat input generates an overshoot, which produce undesirable welded joints. The control of heat input was very important for achieving a suitable welding penetration, preventions of overheating condition and unacceptable welding defects. Moreover, the combinations of these materials are unique, and the precise heat control is essential to perform the stable welding process. In this study, the overlap welding between a FPC, which consist of a thin copper circuit on a polyimide film, and a thick brass electrode by a pulsed Nd:YAG laser were experimentally and numerically investigated with the control of pulse waveform. The numerical analysis was conducted based on the fundamental analysis of the heat transfer problem during the laser micro-welding by finite element method (FEM). The weld strength was also evaluated by shearing test for the overlap welding with and without the control of pulse waveform.

2. Overview of approach

Reflectivity varies depending on the temperature; when a material gets hotter, the absorption of the incident light increases. However, in the case of copper, the high thermal conductivity prevents from getting hotter, thereby maintaining the high reflectivity. Figure 1 shows the absorptivity of copper for 1064 nm wavelength and its thermophysical properties as a function of temperature.[10,11] At room temperature, the absorption rate of the Nd:YAG laser is low, approximately 5 %. It is difficult to obtain a stable laser micro-welding process, since the absorptivity increases drastically. On the other hand, the thermal conductivity decreases when the material reaches its melting point. In other words, when the laser beam is irradiated on the target, its high reflectivity permits only a small absorption of the incident energy. At the same time, the energy absorbed is quickly removed from the interaction point due to the high thermal conductivity. Then, the temperature rises slowly and the formation of the keyhole is consequently delayed. The weld condition of highly reflective materials can be improved with an essential technique of pulse waveform.[12]

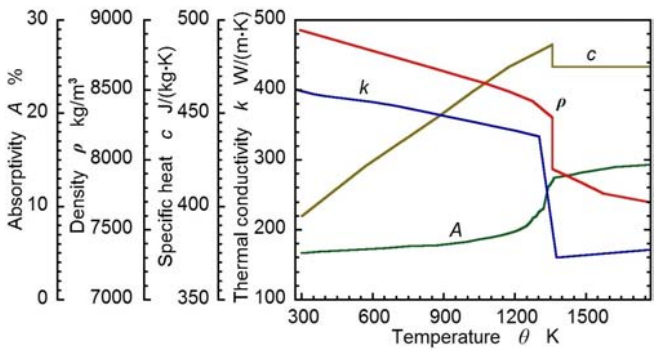

Fig. 1 Thermophysical properties and absorptivity of copper for 1064 nm wavelength

There are several published papers related to the laser welding using pulse waveform technique on the materials with high reflectivity and thermal conductivity such as copper and aluminum. Biro, E. et al.[13] reported that the weld bead quality was improved by the ramp-down pulse waveform in the laser welding of copper. In addition, the controlled heat input by pulse waveform adjustment was effective in controlling the weld behavior of copper.[5] Meanwhile, it has been reported that the laser welding of aluminum alloy was successfully applied with controlled pulse waveform and also to be an effective technique to reduce and eliminate the weld defects.[14,15] With respect to the laser welding with controlled pulse waveform, only a limited number of papers[16-18] have experimentally investigated on the welding of dissimilar materials. However, there are no work have been reported concerning the welding behavior of copper on polyimide and brass in overlap laser welding using controlled pulse waveform. In order to achieve a better understanding into the relationship between the different material properties, complex pulse waveform and its effects on the weld bead, the pulse waveform followed by numerical analysis are strongly required. These points would make the welding of dissimilar materials to a challenging technological problem for applying the laser welding in the industrial application.

In this research, the controlled pulse waveform, which is a technique used to temporally distribute energy within a single laser pulse by controlling the pulse laser power and pulse width in real time was utilized. It can be also defined as a variation in power supplied for a laser to change the shape of the output pulse and subsequently the heat distribution within one pulse. Changing the energy distribution within a pulse can completely change the melting or process behavior of a material. The weld penetration and quality could be improved by changing the laser pulse waveform in these difficult-to-weld applications. Figure 2(a) shows a setting

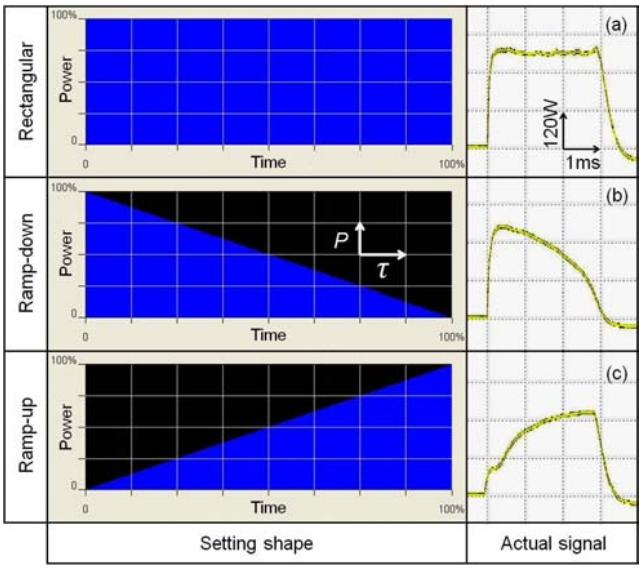

Fig. 2 Setting shape and actual signal of pulse waveform (P=300W, τ=3ms)

profile of a standard laser pulse. This is known as a rectangular pulse waveform with the power densities remaining nominally constant throughout the pulse. Rectangular pulse waveform is the simplest and most extensively used laser pulse waveform containing only one energy sector. Figures 2(b) and (c) show the setting input and actual output of a ramp-down and ramp-up pulse waveforms, respectively. These pulses either emit the majority of their power early or late within the pulse. This equates to either a gradual cooling or gradual heating of material. Materials with dissimilar melting points, a ramp-down pulse waveform reduces weld cracks and porosity.[12] For the latter, materials with low melting points and high reflectivity will benefit from ramp-up pulse waveform during welding. This waveform slowly increases the intensity in weld pulse until much later in the melt.

3. Experimental procedures

A FPC and a brass electrode were used as specimens as shown in Figures 3 and 4, respectively. The FPC, which consists of five layers with four different materials, i.e. adhesive (two layers), polyimide (PI), copper (Cu) and tin (Sn). The sizes of copper circuit were 30 mm length, 2 mm width and 70 μm thickness with the 6 μm tin coating around the copper surfaces, while the adhesive and polyimide layers are 22.5 μm and 25 μm thickness, respectively. The components of brass electrode are copper (70 %) and zinc (30 %). The brass electrode with 650 μm width and 640 μm thickness was also coated with tin layer of 0.01 μm.

A schematic diagram of experimental setup is shown in Figure 5. In this study, a pulsed Nd:YAG laser (LASAG SLS200 CL8) of 1064 nm in wavelength was used as a laser source. The laser beam was delivered by an optical fiber of 50 μm core diameter. The collimator was installed between the optical fiber and the bending mirror, and the focusing point was coordinated by a lens of 50 mm in focal length. In order to avoid the back-reflection of incident laser beam, the processing head was aligned 10 degrees to the perpendicular axis of specimen surface. The specimens were welded in an overlap joint geometry, where the thin copper circuit of FPC overlapped on a brass electrode under a shielding gas of nitrogen with 13 L/min flow rate. The position of laser irradiation was confirmed using a CCD camera located at the top of processing head. The setting shape of pulse waveform was controlled by the computer software, which is connected to the laser source machine. The actual signal of current waveform was measured by the digital oscilloscope, while the actual signal of pulse waveform was monitored and measured by the photodiode. After the laser welding, the sectioned surface of welded specimen was ground, polished and etched for the observation of weld bead by an optical microscope and scanning electron microscope (SEM).

The shear test was carried out to measure the shear strength of the overlap welded joints. A Shimadzu EZ-L test machine was utilized in this test. The cross-head speed was set to 1 mm/min. The specimen was gripped by the clampers, which are placed in the fixture blocks. Then, a shear load was slowly increased at the suitable increments by the mechanical lever system until the welded joint of specimen was fractured.

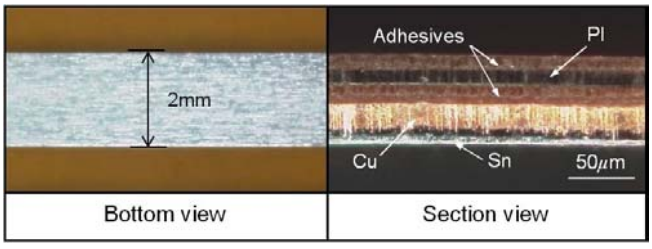

Fig. 3 Photograph of flexible printed circuit

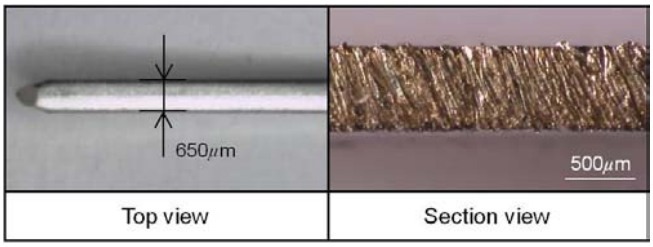

Fig. 4 Photograph of brass electrode

4. Numerical analysis

In this study, the further analysis of the welding phenomenon was conducted by the heat conduction analysis with the finite element method (FEM). The analysis model is based on the fundamental heat transfer for laser micro-welding process. Based on the first law of thermodynamics, the equation for heat flow in a three-dimensional solid can be written as equation (1)[19]

$$\rho \cdot c(\theta)\frac{\delta\theta}{\delta t} = \frac{\delta}{\delta x}\left(k(\theta)\frac{\delta\theta}{\delta x}\right) + \frac{\delta}{\delta y}\left(k(\theta)\frac{\delta\theta}{\delta y}\right) + \frac{\delta}{\delta z}\left(k(\theta)\frac{\delta\theta}{\delta z}\right) + Q_v \quad (1)$$

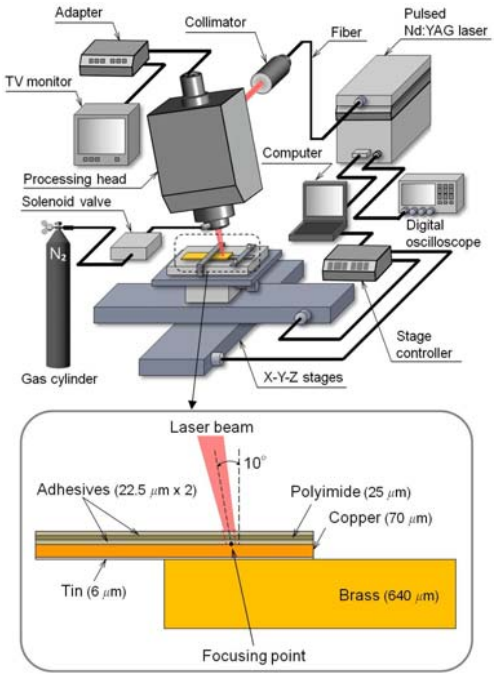

Fig. 5 Schematic diagram of experimental setup

where ρ is the material density, $c(\theta)$ is the temperature dependent specific heat, $k(\theta)$ is the temperature dependent thermal conductivity, Q_v is the volumetric heat source term which varies with a laser power, $\theta = \theta(x,y,z,t)$ is the resulting three-dimensional time dependent temperature distribution in the material, t is time, and x, y, z are the spatial Cartesian coordinates.

Figure 6 shows the developed finite element model, and also shows the magnified mesh view near the interface. Fine mesh resolution is given at and near the heat source, while a fairly coarse mesh density is at the region far from the heat source. A portion of the specimens was designed in the analysis model in order to reduce the calculation time. As the heat source of laser beam is symmetric in the x-z plane, only half the heat source is considered. The heat source comprises a Gaussian plane heat source on the top surface and a conical shape heat source along the thickness of the specimen. To simplify the analysis, the assumption has been made that the alignment of laser spot was perpendicular to the specimen surface. The convective heat transfer condition of air was considered after the set time of laser irradiation. Except for a laser beam irradiated area, the convective heat transfer condition of air was also assumed. The analytical conditions are shown in Table 1. Since the temperature dependent thermal properties are important for the accurate calculation of a temperature distribution. The temperature dependent thermal properties of copper are shown in Figure 1. However, to simplify the analysis the changes in thermal properties with temperature dependent for adhesive, polyimide, tin and brass during laser processing were not considered as shown in Table 2.

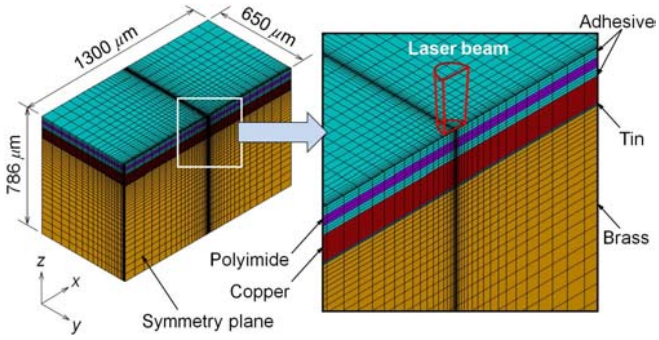

Fig. 6 Finite element model for heat conduction analysis

Table 1 FEM analysis conditions

Parameter/condition	Value
Laser power P W	50 – 400, 500
Pulse width τ ms	3.0, 4.1
Beam diameter d μm	50
Heat transfer coefficient h W/(m²·K)	10
Room temperature θ_{room} K	300

Table 2 Thermal properties for adhesive, polyimide, tin and brass

Material	Thermal conductivity k W/(m·K)	Specific heat c J/(kg·K)	Density ρ kg/m³
Adhesive	0.13	1085	1255
Polyimide	0.14	1090	1380
Tin	67	228	7280
Brass	120	375	8530

5. Results and discussion

5.1 Rectangular pulse waveform

Figure 7 shows the cross-section views for various pulse energies with the rectangular pulse waveform. As shown in the Figure 7(a), the copper layer was not molten at 400 W laser power and 1 ms pulse width (Ep = 400 mJ/pulse). It can be observed that only the brass was molten with the presence of hole due to the lower melting point of brass (1228 K) compared with that of copper (1358 K). Furthermore, since the reflectance of laser beam on a copper is high, the absorbed laser energy is too low to melt a copper. Thus, the molten zone appeared only in the brass at the end of laser pulse. Figure 7(b) shows the cross-section view for higher 500 W laser power and the same 1 ms pulse width (Ep = 500 mJ/pulse). A penetration hole through a copper layer can be observed with the molten region of brass around the hole. In this case, the higher heat input of laser spot would accelerate the evaporation of alloyed zinc in the brass, which has low boiling point (1180 K). The higher laser power enhances to increase the surface temperature of copper and induces more laser energy absorbance. However, this higher laser power resulted in the evaporation at the beginning of laser pulse. Subsequently, for longer 3 ms pulse width with 500 W laser power (Ep = 1500 mJ/pulse) as shown in Figure 7(c), it was clear that the hole became larger due to the long interaction time, which caused the excessive evaporation of alloyed zinc in the brass. From these viewpoints, for joining copper and brass, the 500 W laser power with 1 ms pulse width can be used as a basic model in the thermal analysis.

Figure 8 shows the calculated temperature distributions at the central cross-section of specimen with 500 W laser power and 3 ms pulse width at the time of 1 ms, 2 ms and 3 ms after the beginning of laser irradiation. The evaporation areas of adhesive and polyimide layers were defined as the gray color in the upper part.

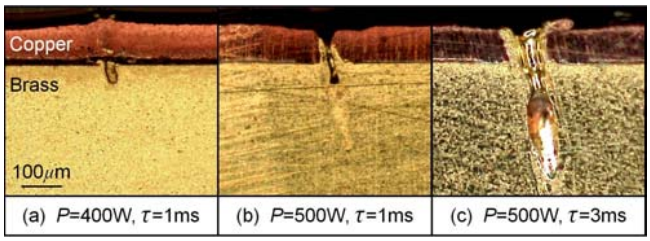

Fig. 7 Cross-section view of welding results with rectangular pulse waveform

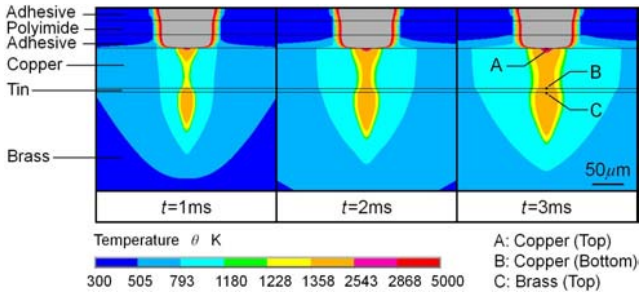

Fig. 8 Spatial temperature distribution at 500W-3ms with rectangular pulse waveform

After the removal of element in the gray color area, the thermal analysis was performed on the outer of evaporation area of adhesive and polyimide layers. It can be seen that the half-bottom of copper does not reach the melting point at 1 ms from the start of laser irradiation. It can be clearly clarified that the absorbed energy on the copper was quickly diffused due to the higher thermal conductivity. In addition, the absorptivity of copper is very low below melting point, which also would make the longer heating time is necessary to rise the temperature from the laser irradiated point of top edge to the bottom edge of copper layer before the joining between copper and brass. Although the laser spot cannot penetrate the copper, the alloyed zinc has reached the boiling point. It can be confirmed that the holes are already formed during this period. Even the longer pulse width increased the temperature to achieve the full-penetration in the copper layer, the size of holes in brass became larger since the energy absorbed was simultaneously increased. In other words, it is considered that the difference in the absorptivity and the specific heat between copper and brass led to the selective evaporation of brass, and a large hole was remained.

Figure 9 shows the temperature history of three points selected in the analysis model, where the points of A, B and C are located at the top edge of copper, at the bottom edge of copper and at top edge of brass as shown in Figure 8, respectively. The red dashed line indicates the melting point of copper. There is an interval time of about 0.8 ms to melt at the bottom edge of copper after the melting of copper at the top edge. Meanwhile, it can be seen that the evaporation of alloyed zinc is growing in point C during that interval time. Alloyed zinc in the brass evaporates easily, and the formation of the hole is inevitable in the laser irradiation with a rectangular pulse waveform.

5.2 Pulse waveform with pre-heating effect

According to the Figure 1, the absorptivity of copper increases approximately three times from the solid state phase at room temperature to the molten phase. Therefore, a solution is to pre-heat the copper that overcome the low initial absorptivity, and it is the most common method used to counteract the high thermal conduction.[20] Based on this point, the pre-heating effect was applied before the joining of FPC and brass electrode on the pulse waveform to prevent from the formation of a large hole. Since the FPC consists of two main layers of thin copper circuit and adhesive/polyimide films, the pre-heating effect was divided into two phases. As shown in Figure 10, the phase 1 is started with lower pulse energy to eliminate the adhesives and polyimide films. This phase also initiates the heat conduction on the copper surface to increase the absorptivity of laser beam. In the phase 2, the higher laser power with an appropriate interaction time is required to generate the molten zone on the copper layer without the melting of brass. It is expected that the phase 2 would prevent from the occurrence of hole in molten area. After the pre-heating effect on the pulse waveform, in the phase 3, the increasing of laser power was employed for joining copper and brass.

The variation of the laser power with time was analyzed by the thermal analysis. Compared with the temperature distributions of the rectangular pulse waveform condition, Figure 11 shows that the temperature rises from the laser irradiated point of top edge to the bottom edge of copper layer. It also can be seen that a sufficient interaction time about 3 ms with 300 W laser power is required to generate the molten zone on the copper layer without melting of brass in the phases 1 and 2. As shown in Figures 11 and 12, the temperature of copper layer rises from the top to the bottom edge of copper layer. It indicates that only the temperature of point C (top surface of brass) rapidly increases during the irradiation time between 3 ms to 3.1 ms in the phase 3, after the full-penetration of the copper layer is achieved. Since the temperature continually increases in the short time, the evaporation of alloyed zinc in the brass could be controlled.

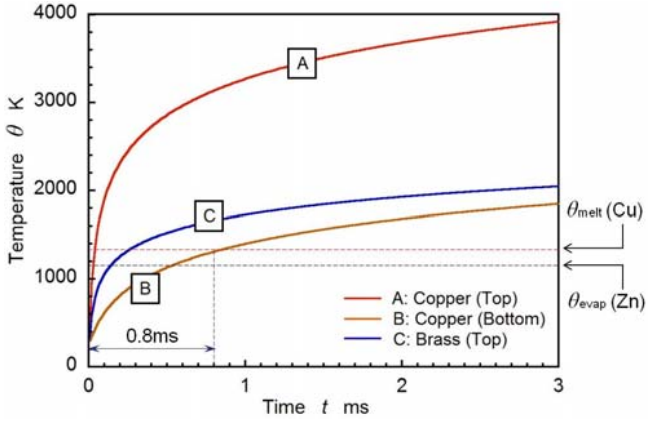

Fig. 9 Temporal temperature distribution at 500W-3ms with rectangular pulse waveform

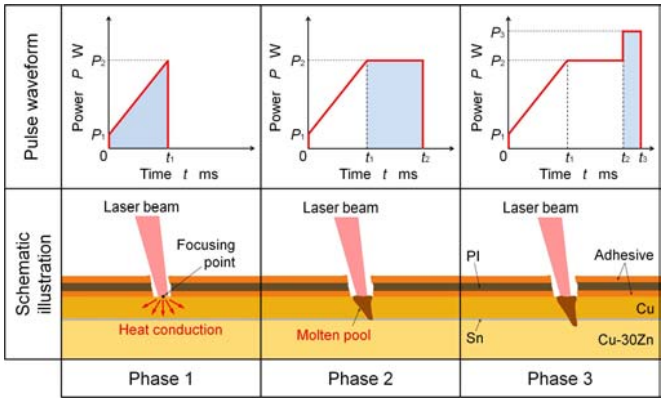

Fig. 10 Schematic illustration of welding mechanism with pre-heating

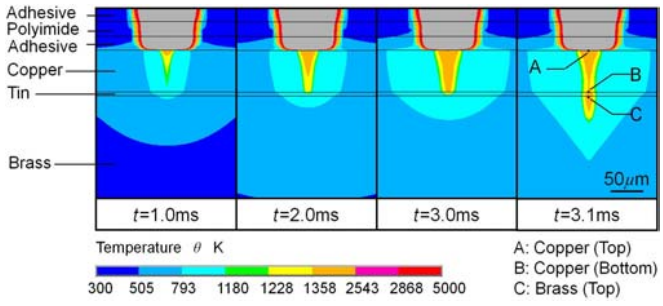

Fig. 11 Spatial temperature distribution with pre-heating effect on pulse waveform

The controlled pulse waveform was divided into three phases including the two phases of pre-heating in the beginning of the pulse. The phase 1 is started with laser power $P1$ up to $P2$ under the duration of pulse width $\tau 1$. $P2$ and $P3$ are the laser powers used in the phase 2 and 3, respectively. The duration of phase 2 is performed with $\tau 2$ of pulse width, while the phase 3 with pulse width $\tau 3$. According to the laser irradiation of the phase 1, which is to remove the adhesive and polyimide films of FPC, the laser power was fixed from 50 W to 300 W and the pulse width were set at 1.5 ms. Figure 13 shows the removal parts of adhesive and polyimide films until the phase 1. It can be observed the top surface of copper at the end of phase 1, and this phase is essential to initiate the heat conduction to increase the absorptivity before the phase 2. The pre-heating effect of pulse waveform in the phase 2 was carried out with the laser power of 300 W, while the pulse width varied from 0.5 to 2.5 ms.

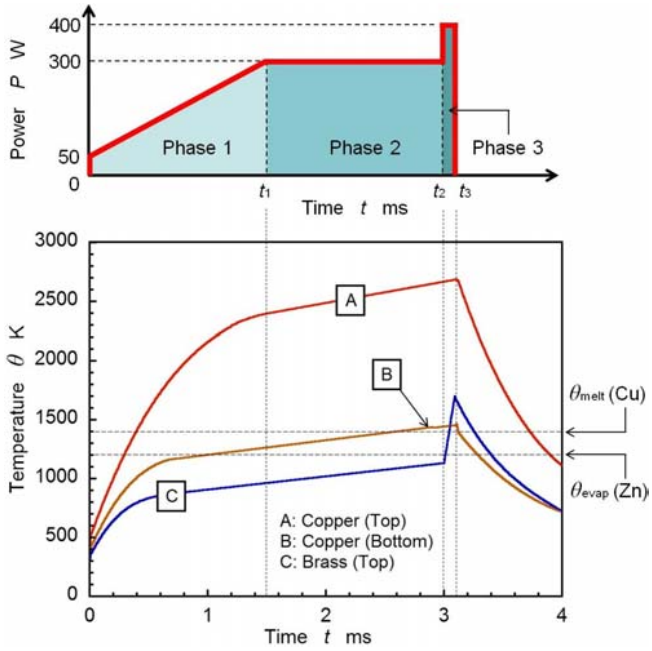

Fig. 12 Temporal temperature distribution with pre-heating effect on pulse waveform

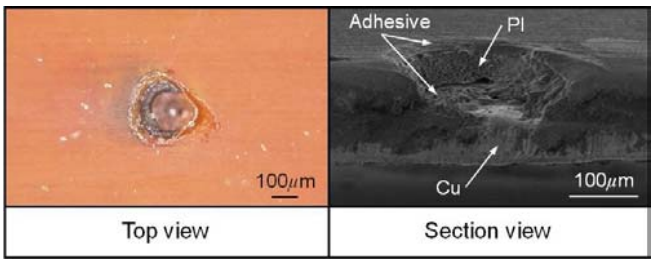

Fig. 13 Removal part of adhesive and polyimide films in phase 1 of controlled pulse waveform ($P1$=50-300W, $\tau 1$=1.5ms)

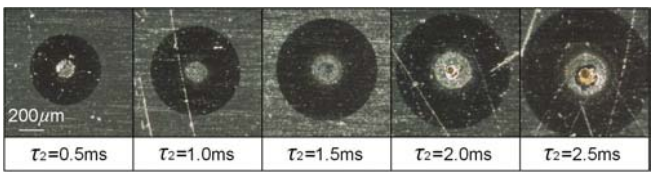

Fig. 14 Bottom view of FPC in phase 2 of pulse waveform with pre-heating effect ($P2$=300W)

Figure 14 shows the bottom views of the FPC until the phase 2. The heat-affected zone and molten zone could not be confirmed from the cross-section view. As can be seen from the inappropriate conditions of 300 W laser power with the irradiation time of 2 ms and 2.5 ms, the laser spot fully penetrated through the copper layer, and the blowhole was generated. From these results, the 300 W laser power with 1.5 ms pulse width is appropriate condition to generate molten zone without the penetration hole for the phase 2 of pulse waveform.

Next, the phase 3 of pulse waveform was carried out for the joining of copper and brass. The laser power and pulse width were set at 400 W and 3.5 ms, respectively. The pulse waveform and cross-section view of welding result are shown in Figure 15. The porosity and bump defects were observed contrary to the expected result. Porosity is formed due to the instantaneously increase of laser power in phase 3. Another cause of porosity is the trapped gases of alloyed zinc from the bottom of the weld keyhole, which is occurred under a high pressure.[21] It can be noted that the high pressure of trapped gasses pushed upward the molten copper to generate bump, and it was solidified immediately at the end of laser pulse. Therefore, the post-heating effect on the pulse waveform was considered for the copper-brass joining without weld defects.

5.3 Pulse waveform with pre- and post-heating effects

The phase 4 of post-heating is a subsequent function of the

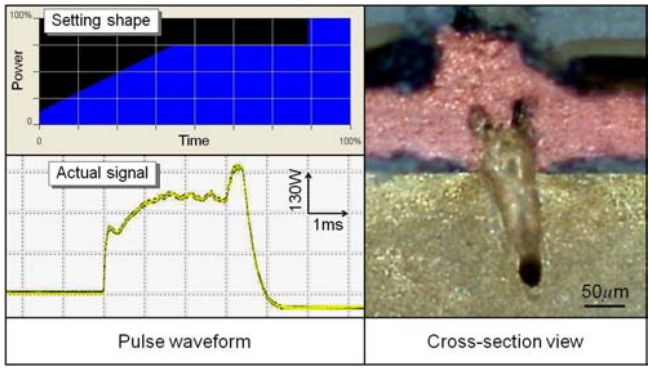

Fig. 15 Welding result of pulse waveform with pre-heating effect (P=400W, τ=3.5ms)

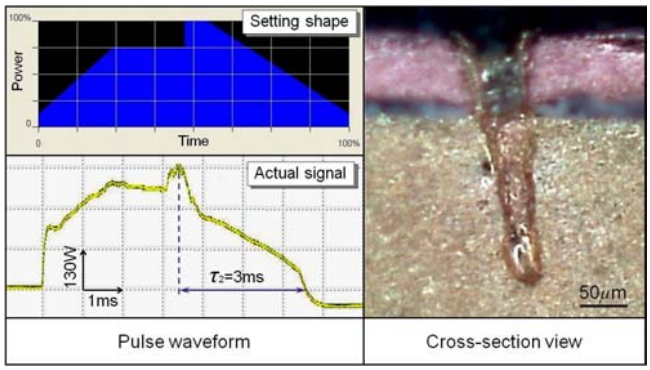

Fig. 16 Welding result of pulse waveform with pre- and post-heating effects (P=400W, τ=6.5ms)

phase 3 by adding the heat to melt the bump generated in phase 3. This re-melting process was intended to fill the hole in order to obtain a better joining condition. Figure 16 shows the configuration of pulse waveform with the pre- and post-heating effect and the cross-section observation. As a new phase 4 in the configuration of pulse waveform, the laser power gradually decreases to stream down the bump below the evaporation point of brass. As a result, it can be seen that the use of post-heating configuration has a positive effect on molten pool to remove the bump. However, the use of longer pulse width ($\tau 4$ = 3 ms) generated an undercut defect on the copper layer. This result would be caused by the overheating, where most of the copper and zinc have been evaporated. Therefore, it is considered that the post-heating should be modulated with small and sustainable heat input by introducing an approach of rest time in the post-heating phase of pulse waveform.

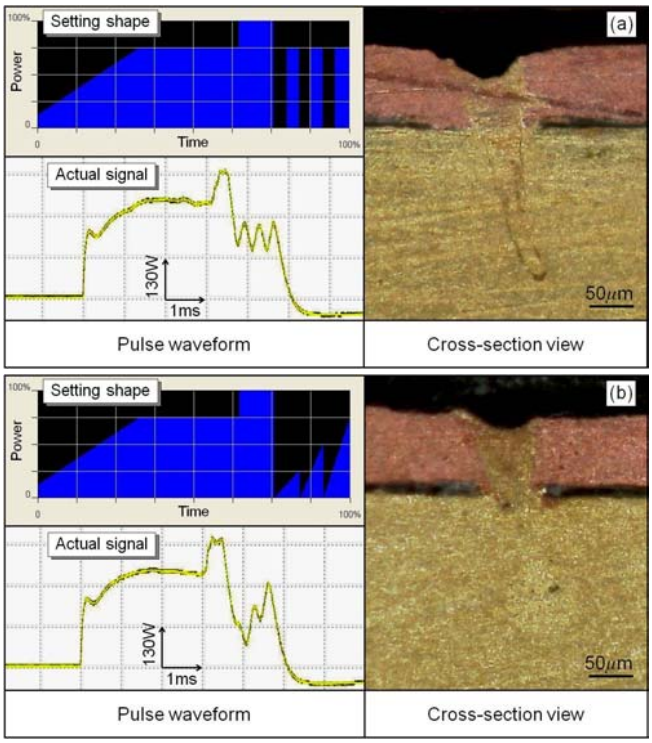

Fig. 17 Welding results of two pulse waveforms with pre- and post-heatings including rest time (P=400W, τ=4.7ms)

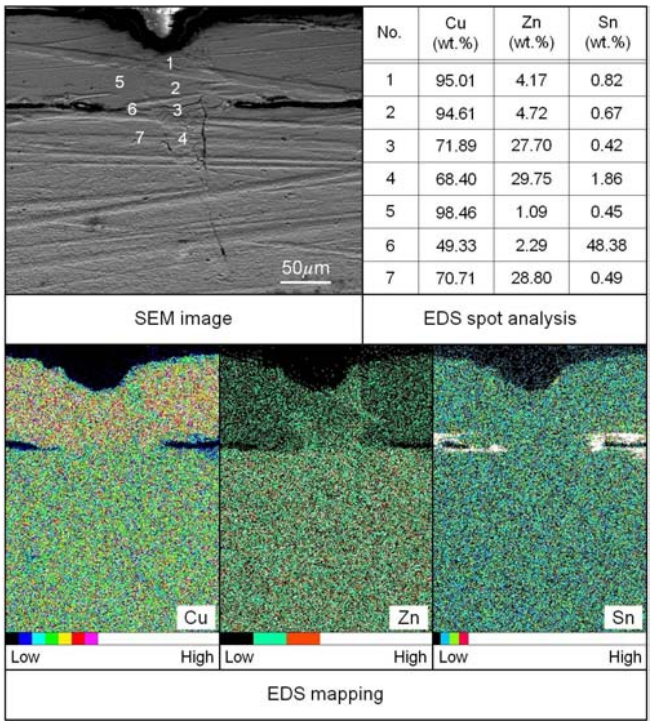

No.	Cu (wt.%)	Zn (wt.%)	Sn (wt.%)
1	95.01	4.17	0.82
2	94.61	4.72	0.67
3	71.89	27.70	0.42
4	68.40	29.75	1.86
5	98.46	1.09	0.45
6	49.33	2.29	48.38
7	70.71	28.80	0.49

Fig. 18 SEM image, EDS analysis and mapping of pulse waveform with pre- and post-heatings including rest time

At the particular time in the post-heating of phase 4, the laser power was set to zero for the reduction of the heat input as shown in Figure 17. The waveform of post-heating is divided into three pulses with the rest time inserted between pulses. It can be noted that the hole was filled without any weld defects in both conditions. It can be proved that an appropriate heat input on the post-heating phase melted the bump and filled the hole in the brass layer. Furthermore, the rest time can be expected to avoid the overheating and to stabilize the weld joint. Therefore, it can be clearly confirmed that the direct joining of a FPC and a brass electrode was realized without any weld defects by the pulse waveform with pre- and post-heating effects including the rest time.

In addition, the elemental analysis was performed to observe the element distribution at the welded parts, such as Cu, Zn and Sn using a scanning electron microscope (SEM) equipped with the energy dispersive spectroscopy (EDS). Figure 18 shows the EDS mapping and spot analysis results of overlap welding by pulse waveform with pre- and post-heatings including rest time (Figure 17(a)). According to the distribution map of element, the small amount of Zn element was uniformly distributed in the molten zone of copper layer. It was confirmed by the EDS spot analysis, where the slightly high percentage of Zn in the molten zone of copper layer (Point 1 and 2) compared than the copper metal away from the molten zone (Point 5). It can be noted that the small amount of Zn element from the brass material of electrode was moved to the top of molten zone during the joining process.

5.4 Evaluation of weld strength

In order to evaluate the weld strength on the overlap welding with and without the control of pulse waveform, the shearing test was carried out. The shearing test was performed at three times for every irradiation condition, and then took the average value.

Figure 19 shows the fracture part on the top surface of brass electrode after the shearing test. It shows that, in the laser welding with the rectangular pulse waveform condition, the fracture occurred with the presence of hole. On the other hand, in the welding with the control of pulse waveform, the fracture occurred without the defect of hole.

Figure 20 shows the various laser pulse waveforms used for the shearing test. As can be seen from Figure 21, it was clear that the shear strength of welded specimen with the rectangular pulse waveform (Case 1-3) showed a lower value than that with the controlled pulse waveform (Case 4-8). As shown in Figures 7 and 19, it could be noticed that the existences of hole and porosity defects had obvious influence on the weakness of weld joint

strength, even if the rectangular pulse waveform generated larger heat input. With the control of pulse waveform, there was decreasing in heat input, while the shear strength increased. The pulse waveform with only pre-heating (Case 4) was less significant on the weld strength, since the bump and porosity defects were occurred on the weld joint as shown in Figure 15. Compared with the pulse waveform with the pre- and post-heatings, the insertion of rest time on the post-heating phase is expected to avoid the overheating and weld defects. It showed the higher shear strength, even it yields smaller welded joint area. However, it shows that the pulse waveform with the pre- and post-heatings of Case 7 and 8 were less significant to increase the weld strength. It can be noted that the inappropriate pulse shape on the post-heating phase was directly affected on the lower weld strength. Therefore, it is clearly that the appropriate controlled laser pulse configurations are effective to produce a higher strength of joint for a direct joining between a FPC and a brass electrode.

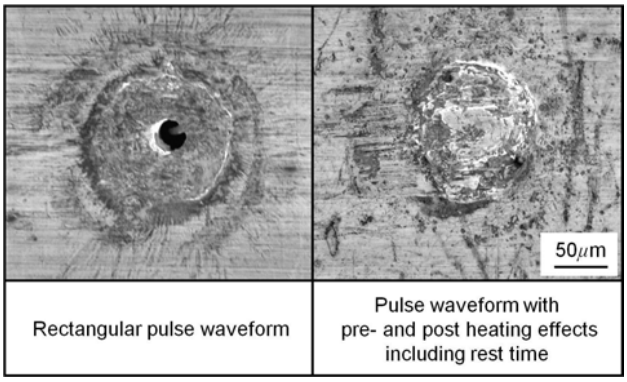

Fig. 19 Fracture on the top of brass electrode

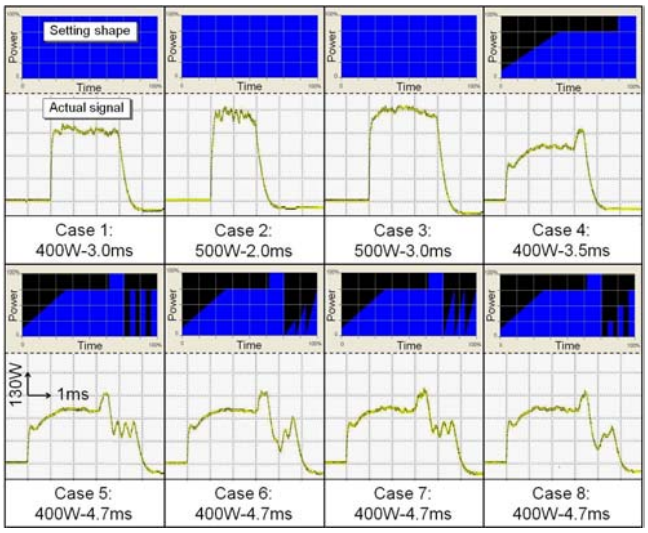

Fig. 20 Pulse waveforms used for the shearing test

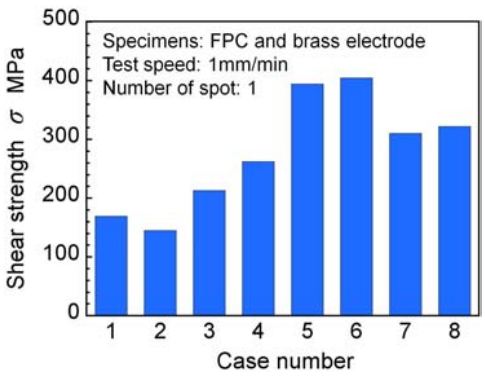

Fig. 21 Shear strength of the welding with and without the control of pulse waveform

6. Conclusions

The overlap welding of thin copper circuit and thick brass electrode by using the control of pulse waveform and heat input was experimentally and numerically investigated. Main conclusions obtained in this study are as follows:

- Alloyed zinc in the brass was evaporated easily, and the formation of porosity was inevitable in the laser irradiation with the rectangular pulse waveform.
- Pre-heating effect of the pulse waveform was essential to increase the surface temperature of copper and induced higher absorption of laser energy at the beginning of laser pulse.
- Post-heating effect of the pulse waveform performed a positive result to remove the bump defect. However, the inappropriate heat input led to the undercut defect in copper layer.
- Better weld joint without weld defects could be achieved by adding a rest time in the post-heating phase.
- The higher shear strength could be obtained by the control of pulse waveform to perform the good joining without weld defects.

REFERENCES

1. Katayama, S. and Kawahito, Y., "Laser Direct Joining of Metal and Plastic," Scripta Materialia, Vol. 59, No. 12, pp. 1247-1250, 2008.
2. Ozeki, Y., Inoue, T., Tamaki, T., Yamaguchi, H., Onda, S., Watanabe, W., Sano, T., Nishiuchi, S., Hirose, A. and Itoh, K., "Direct Welding between Copper and Glass Substrates with Femtosecond Laser Pulses," Applied Physics Express, Vol. 1, Paper No. 082601, 2008.
3. Kim, J.-W. and Kim, C.-G., "Design of a Laser Welded Thin Metal Tube Structure Incorporating Welding Distortion and Residual Stress," Int. J. Precis. Eng. Manuf., Vol. 11, No. 6, pp. 925-930, 2010.
4. Otte, F., Stute, U. and Ostendorf, A., "Micro Welding of Electronic Components with 532nm Laser Radiation," Proc. of SPIE, Vol. 6458, Paper No. 645804, 2007.
5. Takahashi, K., Watanabe, T., Matsusaka, S. and Wada, T., "Direct Microjoining of Copper Materials using Laser Beams," JSME International Journal Series C, Vol. 49, No. 1, pp. 128-134, 2006.

6. Shannon, G. and Severloh, P., "Laser Microwelding of Copper," Industrial Laser Solutions, pp. 1-3, 2009.
7. American Welding Society, "Welding Copper and Copper Alloys," pp. 10-13, 1997.
8. Migliore, L., "Laser Materials Processing," Marcel Dekker, pp. 176-178, 1996.
9. Ion, J. C., "Laser Processing of Engineering Materials," Butterworth-Heinemann, pp. 431-433, 2005.
10. Blom, A., Dunias, P., Van Engen, P., Hoving, W. and De Kramer, J., "Process Spread Reduction of Laser Microspot Welding of Thin Copper Parts Using Real-time Control," Proc. of SPIE, Vol. 4977, pp. 493-507, 2003.
11. Japan Society of Thermophysical Properties, "Thermophysical Properties Handbook," pp. 23-25, 2008.
12. Naeem, M., "Controlling the Pulse in Laser Welding," Welding, pp. 1-4, 2004.
13. Biro, E., Weckman, D. C. and Zhou, Y., "Pulsed Nd:YAG Laser Welding of Copper Using Oxygenated Assist Gases," Metallurgical and Materials Transactions A, Vol. 33, No. 7, pp. 2019-2030, 2002.
14. Rohde, M., Markert, C. and Pfleging, W., "Laser Micro-Welding of Aluminum Alloys: Experimental Studies and Numerical Modeling," Int. J. Adv. Manuf. Technol., Vol. 50, No. 1-4, pp. 207-215, 2010.
15. Zhang, J., Weckman, D. C. and Zhou, Y., "Effect of Temporal Pulse Shaping on Cracking Susceptibility of 6061-T6 Aluminum Nd:YAG Laser Welds," Welding Journal, Vol. 87, No. 1, pp. 18s-30s, 2008.
16. Schmidt, M. and Weigl, M., "Laser-Bonding in High Power Electronics," Journal of Laser Micro/Nanoengineering, Vol. 5, No. 3, pp. 242-247, 2010.
17. Witte, R., Liebers, R., Holtz, R., Wilden, J. and Neumann, T., "Laser Welding with Pulsed Solid State Lasers: Strategies and New Developments," Proc. of the 11th International Symposium on Laser Precision Microfabrication, Paper No. 10-75, 2010.
18. Naeem, M., Lewis, S. and Chinn, J., "Microwelding Performance Comparison Between a Lower Power (125W) Pulsed Nd:YAG Laser and a Low Power (100-200W) Single Mode Fiber Laser," Proc. of the 3rd Pacific Int. Conf. on Applications of Lasers and Optics, pp. 721-726, 2008.
19. Kannatey-Asibu, E., "Principles of Laser Materials Processing," John Wiley & Sons, pp. 232-235, 2009.
20. Duley, W. W., "Laser Welding," John Wiley & Sons, pp. 25-27, 1999.
21. Laser Institute of America, "LIA Handbook of Laser Materials Processing," pp. 320-322, 2001.